Synthesis and Activity of A Single Active Site N-doped Electro-catalyst for Oxygen Reduction

Maryam Bayati and Keith Scott*

AUTHOR ADDRESS Department of Chemical Engineering and Advanced Materials, Newcastle University, Newcastle upon Tyne, UK

KEYWORDS N-doped carbon, oxygen reduction reaction, Iron inserted nitrogen doped carbon, graphitic nitrogen, quaternary nitrogen and active site.

ABSTRACT Nitrogen doped carbon materials are promising oxygen reduction reaction (ORR) catalysts which could potentially replace platinum. However, despite extensive studies, their active sites are still controversial and their impact on overall ORR remains obscure. Herein, we present a method for preparation of a single active site catalyst based on cycling an iron-inserted N-doped carbon catalyst in a wide potential window firstly in sulfuric acid and later in alkaline solution to study the contribution of the remaining one active group in overall activity. Following preparation of the metal-inserted N-doped carbon catalyst (MINC), its morphology was characterized using X-ray photoelectron spectroscopy (XPS), high resolution transmission electron microscopy (HRTEM), X-ray diffraction (XRD), and the electro-catalytic behavior was investigated by employing linear sweep voltammetry (LSV) using a rotating ring disk electrode (RRDE). XPS revealed that graphitic nitrogen was the only remaining active nitrogen-containing group after elimination the pyridinic and pyrrolic groups and also iron nano-materials removal confirmed from

auger peak of Fe LMMa and poisoning reaction with cyanide. The C1s XPS region data showed an increase in the oxygen reduction intermediate C-OH peak, after the reaction, which indicates electrocatalytic activity of the graphitic carbon. Electrochemical studies revealed no significant changes in limiting current, a small increase in H_2O_2 production and 47 mV shift in half wave potential for degraded catalyst which is in line with previous theoretical calculations.

1. INTRODUCTION

The depletion of energy resources and environmental pollution are urgent problems in contemporary society[1].Low-temperature, polymer electrolyte fuel cells(PEFC) have been recognized as clean energy-converting devices due to their high efficiency, low/zero emissions, for applications in small electronic devices, residential power generation and transportation, which makes them a promising technology to combat the above mentioned global challenges. However, major technical challenges which limit the commercialization of PEFCs are the precious metal based catalyst cost, catalyst poisoning and limited durability. Consequently, employing non precious-metal catalysts would be of great benefit in accelerating commercialization of PEFCs. Several types of non-precious metal (NPM) catalysts have been explored including; transition metal chalcogen materials, pyrolyzed macrocyclic compounds and doped carbon compounds[2]. Amongst these, doped carbon material, with and without non-precious metals, have shown promise as catalysts for ORR; providing the benefits of low price due to use of earth abundant compounds as precursors. Investigation on this class of catalyst commenced with Jasinski`s work[3] and the catalyst efficiency and longevity was improved by employing various precursors at elevated temperatures. Recently synthesized Fe (and/or Co)-N-doped carbon catalysts showed onset potentials and durability comparable with state of the art Pt[4]. Despite these progresses, the active

centers in the nitrogen doped compounds need to be identified for further understanding of ORR. This will help in guiding the synthesis of materials with improved activity, stability, and selectivity. It has been debated that nitrogen, in various oxidation states and configurations, metal-N moieties, the latter in vicinity of metal nanoparticles or on the contrary without metal nanoparticles, carbon in vicinity of the N-doped atomdue to its induced positive charge or its basicity, vacancy defects or a combination of several of them, depending on media and catalyst structure, are the source of the activity[5]. Considering that no synthesis methods, so far, has resulted in an ideal single active site catalysts, therefore indirect methods, poisoning selected active sites,hypothesis and theoretical models being employed to simplify the overall scenario and provide insight into the mechanism and nature of each individual site[6,5L,5J,5I]. The theoretical calculation, still cannot explain a complex multi-active center catalyst behavior. Therefore, preparation of catalysts with only one kind of active site is considered an ideal route to understand catalyst behavior. Herein, for the first time, to our knowledge, we have used a post-synthesis degradation method to achieve this goal. To do this, a highly active MINC catalyst was degraded following the synthesis by potential cycling in sulfuric acid and then in KOH solution to remove metal contents and less stable N-functionalities and leave only one active functional group for the ORR. It is shown that electrochemical cycling the catalyst lower than the redox potential of iron (E^o (Fe^{III}/Fe^{II})=0.77 V_{RHE}) results in removal of iron nanoparticles via reductive dissolution mechanism in acid media and radicals produced during ORR oxidize Fe-N moieties.[5M] Therefore to remove iron-content active sites, the catalyst initially cycled in 0.5 M sulfuric acid followed by cycling in 0.1 M NaOH under oxygen. The resultant material was characterized morphologically and electrochemically to understand and correlate the role of the active site with the overall performance.

2. EXPERIMENTAL SECTION

2.1. Materials and Instrumentation

The electrochemical measurements were carried out with an Autolab potentiostat, PGSTAT302N, Methrohm Autolab B. V. A platinum coil was used as the counter electrode; the potentials were measured and are reported with respect to a silver/silver chloride reference electrode (3 M NaCl) (for ease of comparison in 0.1 M NaOH, $E_{RHE}=E_{Ag/AgCl,\ 3M\ NaCl}+0.977$ V). All measurements were performed at a temperature of, 22 ± 2 ºC. The electrochemical experiments for ORR were conducted in O_2 saturated 0.1 M NaOH solution. Solutions were prepared with de-ionized water and purged with nitrogen (BOC, 99.998%) for 20 min before each experiment, saturated with oxygen during ORR (BOC, 99.998%) and kept a blanket of it during the experiments. A three-electrode cell was employed for the electrochemical measurements on a rotating GC disk with Pt ring electrode from ALS Co., Japan. The electrode was cleaned initially by polishing with alumina powder (1.0, 0.3 and 0.05 μm diameter, Buehler® GmbH, Germany) on a cotton wool polishing cloth (Buehler® GmbH, Germany) and rinsed with de-ionized water. The cleaning procedure was followed by sonication in water for 20 min and repeated before each electrochemical measurement. The electrode was prepared by mixing 10 mg of catalyst, 2.25 ml of de-ionized water/ethanol and 0.25 ml of 5% Nafion 117 solution in an ultrasonic bath and placing the required amounts of the catalyst suspension on the mirror-polished glassy carbon disk to dry (loading= 0.3 mg cm^{-2}). The catalyst was degraded by cycling between 1 to zero V vs. Ag/AgCl 3M NaCl, in 0.5 M sulphuric acid 20 times (scan rate=10 mVs^{-1}) then between 0.1 to -0.9 V vs. Ag/AgCl in 0.1 M NaOH solution 7200 times at 50 mVs^{-1}scan rate in an oxygen saturated atmosphere. Photoelectron spectra were recorded with a K-Alpha spectrometer (NEXUS, Newcastle University, UK) employing an Al Kα X-ray source. The spectra were collected with a pass energy of 20 eV, which is typical for

high-resolution conditions. The binding energies (BEs) were referenced to the C 1s peak. Nafion peaks have been subtracted from elemental region of XPS spectra of the degraded sample by using the non-overlapping, strong C1s peak of nafion located at very high energy of around 292 eV. The overlapped peaks have been subtracted proportional to this peak as it has been described by Xing[12A]. High resolution transmission electron microscopy (HRTEM) measurements were conducted with a 200 KV Phillips CM200 FEGTEM equipped with an Oxford Instruments INCA 350 EDX system/80mm X-Max SDD detector. Specimens for HRTEM measurements were prepared by depositing a droplet of nanoparticles suspension on a 400 mesh copper grid coated with a holy carbon film and then evaporating the solvent in air at room temperature. XRD was recorded on a PAN analytical X'Pert Pro MPD diffractometer using Cu Kα radiation. CHN analysis was carried out with a Carlo Erba 1108 Elemental Analyser and controlled with Carlo Erba Eager 200 software.

Cyanamide (Aldrich, 99.0%), Potassium cyanide (Sigma-Aldrich, >97%), iron(II) acetate (Sigma-Aldrich, 99.99%), black pearl2000 (BP2000) (CABOT), absolute ethanol (Fisher Scientific), nitric acid (Sigma-Aldrich, 70%), sulphuric acid (Sigma-Aldrich, 99.99%) and sodium hydroxide (Sigma-Aldrich, 99%) were used as received.

2.2. Synthesis of the Catalyst

Black pearl (BP) as carbon support was partially oxidized by 70% nitric acid at 80◦C.The oxidized material was separated using a centrifuge equipment, rinsed thoroughly with de-ionized water up to neutral PH and dried in an oven at 80◦C. 1 g of oxidized BP was added to a stirring solution of cyanimide and iron acetate in ethanol in a ratio of 3.5/1 at 60◦C. Following evaporation of the solvent, it was pyrolyzed at 950C for one hour in an inert atmosphere of N_2, leached in 0.5 M

sulphuric acid solution for 8 h at 80 °C to remove the excess amount of iron and heat-treated at 950 °C for one hour in N_2 atmosphere.

3. RESULTS AND DISCUSSION

Figure 1 shows high resolution transmission electron microscopy (HRTEM) images of the synthesized catalyst at three magnifications. The lowest magnification micrograph (Figure 1I) shows an irregular shape of nanofiber composite consistent of iron compound nanoparticles encapsulated in carbon onion-like shells (Figure 1II). This composite has been supported on oxidized carbon BP 2000 and its irregular structure can be seen in the top right corner of the micrograph. The inter-layer spacing of the shell is 0.34 nm, which is very close to the size of single-crystal graphite (0.335 nm) representing C(002) encapsulating iron nanoparticles with lattice constant of 0.287 nm presenting the formation of α-Fe(110) (Figure 1III). CHN analysis of the synthesized catalyst shows 1.6% nitrogen while surface elemental analysis by X-ray photoelectron spectroscopy (XPS) (see Table1) displays approximately twice that amount (3.8% average for ten samples) indicating that N-doped carbon is formed on the surface of the carbon support than doping the bulk carbon.

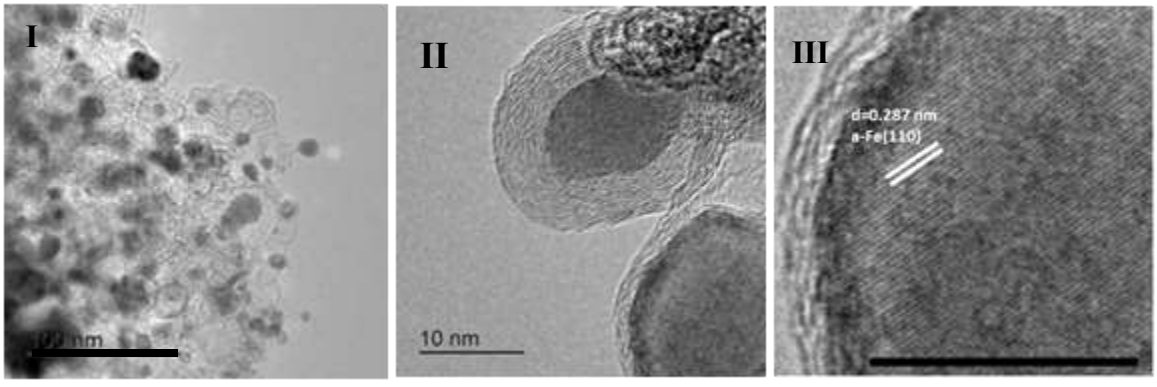

Figure 1. HRTEM image of as-prepared catalyst at low (Scale= 100 nm) (I), high (II) magnifications and lattice fringes of α-Fe(110) (III) (Scale= 10 nm).

Table 1. XPS elemental analysis of the synthesized and degraded catalysts.

Elements	N	C	Fe	O
%Atom in as-synthesized catalyst	3.77	93.51	0.28	2.44
%Atom in degraded catalyst[b] [a]	2.14	81.64	0	16.23

[a] Results after subtracting nafion contribution. [b] Details in tableS1.

The structure and phase composition of the catalyst were characterized by X-ray diffraction (XRD) (Figure 2). The diffractogram shows a broad peak at 24.9°, superimposed on a sharp peak at 25.7°, correspond to graphite (002), and the formation of large domains of a highly ordered carbon structure with a calculated interlayer space of 0.34 nm (for pristine graphene). The peak at 25.7°, with a d spacing of 0.346 nm, confirmed by HRTEM images, is characteristic of interplanar stacking of aromatic systems in graphitic materials as obtained for nonporous carbon nitrides in a turbo-stratic form[8].The composition of the metal core nanoparticles confirms oxide (Fe_3O_4, orange colour in Figure 2), carbide ($Fe_{15.1}C$, green colour in Figure 2) and metal core (red colour in Figure 2) formation. The diffraction peaks at 35.4°and 43.1°are indexed as (311) and (400) of face-centered cubic (fcc) Fe_3O_4 (JCPDS no. 19-0629), respectively[8].The peaks at 43.4°, 50.7° and 74.7° are assigned to the (111), (200) and (220) planes of austenite ($Fe_{15.1}C$) respectively. The diffraction peaks of iron fcc phase was observed with the calculated lattice constant of 2.862Å, which is very close to reported data (a = 2.860Å, JCPDS file no. 87-0721) and which is consistent with HRTEM (Vida ultra).

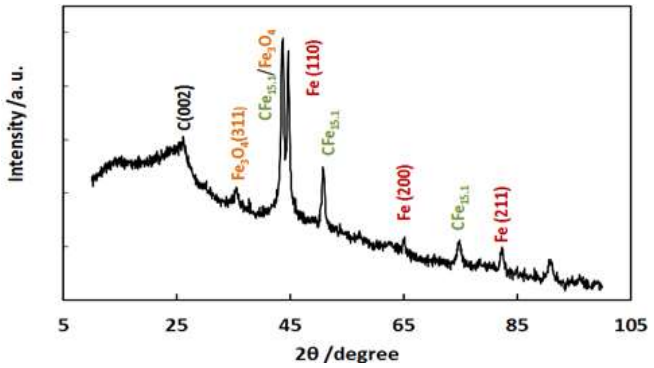

Figure 2. XRD pattern of as-synthesized catalyst.

XPS measurements were conducted to elucidate the chemical composition and element bonding configurations in the as-prepared and degraded catalysts. The survey spectrum of the as-prepared catalyst (Figure S2) reveals the presence of C, N, O and Fe elements. The N 1s spectra deconvoluted into four peaks (Figure 3I-A); assignable to the pyridinic (398.3 eV), graphitic (quaternary) (401.0 eV), pyrrolic (399.6 eV) and oxidized N (402.2 eV)[9] indicate incorporation of the nitrogen atoms into the carbon matrix and therefore enhanced ORR catalytic activity due to induced electronic effects[10]. The peaks at a binding energy of 399.6 eV may have a contribution from nitrogen bound to iron[10C] which considered one of the possible active sites[5F,5J,5L,5I,6D]. Deconvolution of the Fe 2p region revealed a combination of iron in its zero oxidation state and iron oxide[11,10C](Figure 3II-A), confirming XRD and TEM results.

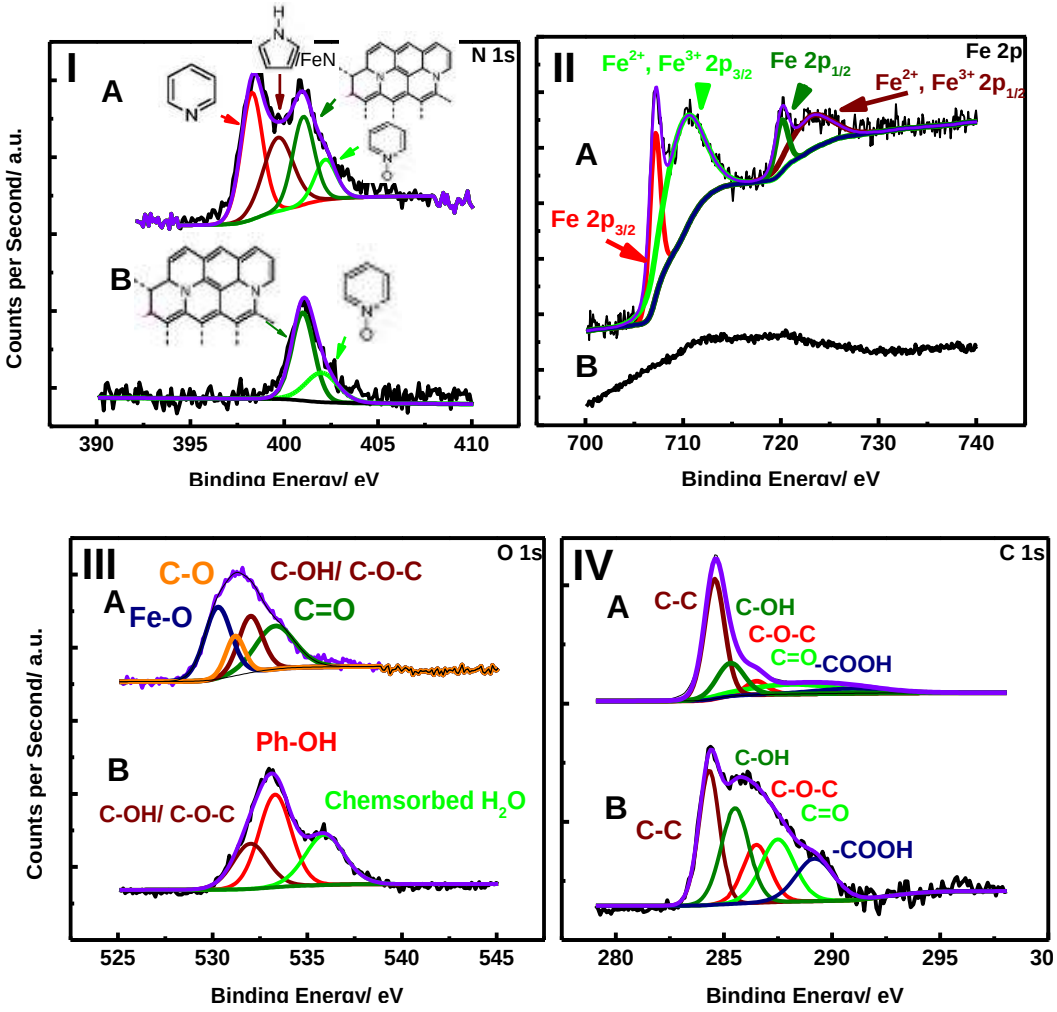

Figure 3. I) Nitrogen 1s, II) Iron 2p, III) Oxygen 1s and IV) carbon 1s XPS spectra of as-prepared catalyst before (A) and after (B) the degradation test. The inserted text colour matches the corresponding peak colour. Y axis presents different scales for A and B spectra.

It can be seen that degradation by potential cycling results in removal of pyridinic and pyrrolic (or/and Fe-N) functionalities (Figure 3I-B) and concurrently in the iron content (Figures 3II-B and III-B) leaving only a background which overlapping with in-elastic scattering of fluorine from nafion ink (Figure S2-red line). Similar background was observed in a control XPS experiment on a Fe-free carbon-nafion mixture (Figure S3). Moreover, the full width, at half maximum (FWHM) of the quaternary nitrogen in N1s region remains the same before and after degradation (Figure3I). Reject the idea of shifting the pyridinic and pyrrolic peaks to high binding energy of 400 eV upon

hydroxylation of the vicinity carbon or protonation of pyridinic functionality at this study[12]. However the latter is less probable because of the alkalinity of the final media. This is possibly due to the fact that pyrrolic and pyridinic nitrogen functionalities are more prone to oxidation than the quaternary functionalities and also that the pyrrolic functionality is prone to conversion to other nitrogen functionalities upon applying high energy[13]. Pyridinic group can be oxidized using hydrogen peroxide to pyridine N-oxide in acid media or convert to graphitic nitrogen via ring-opening procedure during ORR.[13A] The enhancement in oxygen-containing functionalities and quaternary N, in degraded catalyst (Table 1 and S1) indicate oxidation and possible partially inter-conversion of other N-functionalities to quaternary nitrogen. This observation is in line with increases in carbonyl and carboxyl functionalities in the C1s region as a result of degradation. The remaining quaternary nitrogen can exist as in-plane or at the edge in armchair or zigzag configurations[6e]. Since iron compounds considered as active sites at ORR and to remove any doubt and ensure iron removal from the ink upon degradation, two investigations were carried out. Firstly, auger region of iron at 786.7 eV with no overlapping with other elements, was recorded at higher resolution (18 times higher acquisition beam time) and secondly, ORR was conducted in presence of cyanide (*vida infra*).

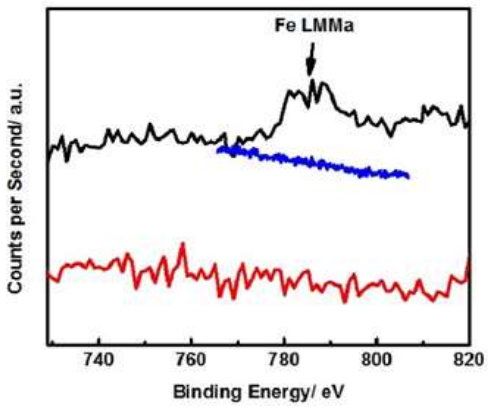

Figure 4.XPS LMMa auger region spectra of Fe for as-synthesized (black line), degraded ink catalyst (red line) and the latter with 18 time higher acquisition time (blue line).

Figure 4 reveals only a flat background and elimination of Fe LMMa peak after the cycling degradation (red and blue lines). The O1s region XPS results confirm elimination of iron components (Figure 3IIIB). Oxygen and carbon XPS regions (Figures 3IIIB and 3IV-B respectively) display an increase in hydroxyl group as an intermediate of the 4e ORR path, after the reaction, which indicates activity of the catalyst after degradation. The analysis of the C 1s spectrum (Figure 3IV-A) shows five peaks centred at 284.6, 285.4, 286.5, 288.1, and 290.8 eV, which are associated with carbon-carbon /carbon-hydrogen, C-OH, C-O-C, carbonyl and carboxyl functional groups respectively[12a], with carbon at its zero oxidation state as the main component. To shed light on electrocatalytic behaviour of the single active site catalyst, electrochemical activity of the as-synthesized and degraded catalysts for ORR was measured using a rotating ring disk electrode (Figure 5I and 5II respectively). RRDE voltammetry was operated at different rotation rates, in 0.1M NaOH and compared with state of the art, commercial 20% Pt/C catalyst (Figure 5III, black line).

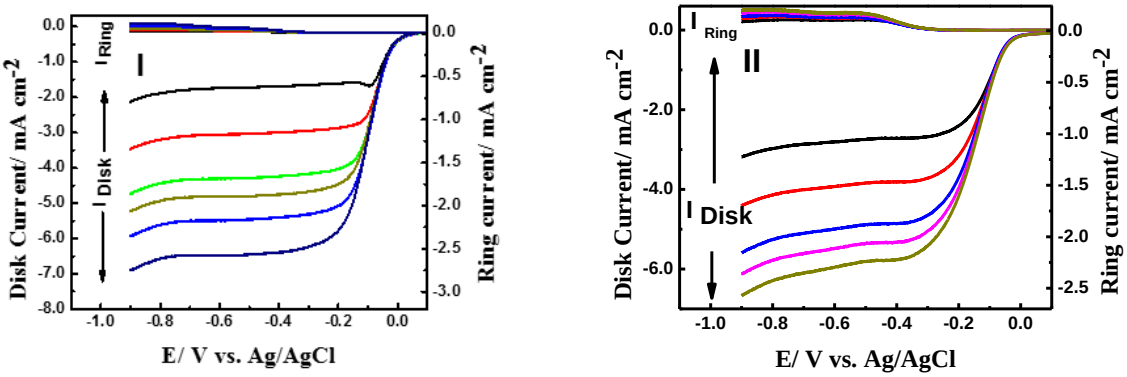

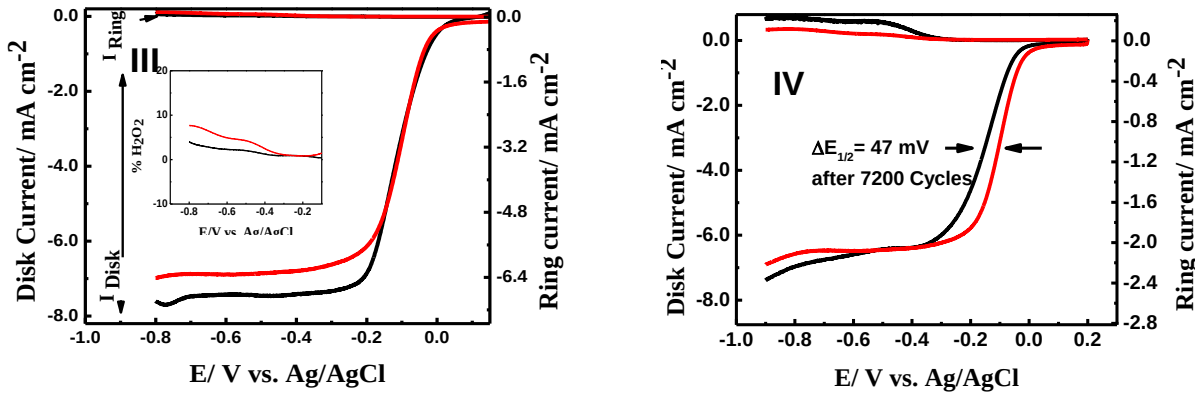

Figure 5. RRDE voltammetric responses for ORR in oxygen saturated solution of 0.1 M NaOH (scan rate=10 mVs^{-1}). The electrode rotation rate was 100, 400, 900, 1600, 2025 and 2500 rpm and Pt ring electrode was polarized at 0.35 V for as-synthesized (I) and degraded (II) catalysts. III) Polarization graphs of as-synthesized (red) and 20% Pt/C (black) at rotation rate of 2500 rpm (Inset shows produced H_2O_2%). IV) Polarization curvess of as-synthesized (red), degraded (black) catalysts at 2500 rpm.

A small shoulder observed around -0.1 V at low rotation rate in the polarization curve for as-synthesized catalyst can be associated to the Fe^{II}/Fe^{III} redox transition or/and a carbanion as the active site for the 4e reduction (Figure 5I)[5F-5G,6D]. A cyclic voltammogram of the catalyst recorded under nitrogen atmosphere reveals broad redox peaks at potential near to iron and/or carbanion redox regions suggesting that either or a combination of these reactions may involve in activating the oxygen and initiating the ORR (Figure S4). Figure 5III shows a comparable ORR activity of the as-synthesized catalyst with Pt. The electron transfer number (n) was determined from the RRDE results on the basis of the following Koutecky−Levich equation:

$$\frac{1}{i} = \frac{1}{i_k} + \frac{1}{\left(0.62nFD^{(2/3)}Av^{(-1/6)}\omega^{0.5}\right)} \qquad (1)$$

The n, and hydrogen peroxide yield (H_2O_2%) are confirmed and obtained respectively from the following equations:

$$n = \frac{-4i_d}{\left(-i_d + \frac{i_r}{N}\right)} \qquad (2)$$

$$H_2O_2\% = \frac{\left(\frac{2i_r}{N}\right)}{\left(-i_d + \frac{i_r}{N}\right)} \times 100\% \qquad (3)$$

Where i_d, i_r and N are the disk-, ring-currents and the collection efficiency (=44% in our experiments) respectively. The amount of hydrogen peroxide produced by the catalyst is at its highest of 7% (n=3.9) while for Pt, it is slightly lower, approximately 4% (Figure 5III, Inset). Although the graphitic carbon has defects caused by doping and oxidation, it can be seen that its resistance is comparable to 20% Pt/C; which is paramount in fuel cell applications. By correlating the ORR measurements with the XPS analysis, the high activity of the as-synthesized catalyst can be attributed to the active sites of iron-content, pyridinic, quaternary and pyrrolic groups, which is in agreement with previous reports[6, 12]. Upon degradation of the catalyst, the activity declined and the half-wave potential shifts 47 mV toward a lower potential (Figure 5IV) which is nearly half that for Pt/C (Figure S5). No significant changes were observed in the limiting current after the potential cycling. Figure 5II shows the ORR electro-catalytic performance for degraded catalyst and it is clear that the catalyst is still very active. To further investigate into the possible remaining of Fe-N_x active sites, the degraded catalyst was poisoned with CN^- ion in 0.1 M NaOH solution and under oxygen (Figure S6). Cyanide solution was chosen over SCN^- because its higher affinity for iron centre.[5J] Presence of cyanide did not show any remarkable poisoning effect on the ORR activity and confirmed the XPS results in removal of iron active centres. According to XPS results and since there is no report of nitrogen-oxide activity for ORR, it is concluded that the only source of activity is quaternary N-doped carbon. This is, to our knowledge, the first time observation of the, quaternary N-doped carbon activity for ORR and thus sheds some light on the long-time debate over its electro-activity. These findings are in line and confirming the theoretical modelling that the pyridinic and the N-graphitic functionalities offer high activity for ORR even in absence of

metal centre[6e]. It has been shown that the total number of pyridinic and graphitic N (Table S1) and concurrently the limiting current remains, effectively, unchanged after degradation, which is consistent with Subramanian conclusion that both pyridinic and graphitic nitrogen activate the ORR process via the 4e path-way[14]. Lai *et al.* showed that Pyridinic N contributed in improving the thermodynamic barrier whereas the quaternary nitrogen could enhance the kinetic performance and regulate the limiting current[15] and explains the observed shift in onset potential. The latter is also in line with Sharifi`sresults.[16] Our results are supported by theoretical calculation for activity of quaternary N-doped carbon in zigzag or armchair configurations[4c,6a,6b,6e]and some conclusions from experimental data[16]. Saidi`s DFT calculation for N-doped graphene quantum dots showed that the pyridinic-type nitrogen doped has the smallest over-potential for 4e ORR pathway, while the onset of graphitic-type N-doped quantum dot appears at least 35 mV lower potential[6b] which is in accordance to our experimental findings. As the result of oxidizing and inter-conversion of pyridinic and pyrrolic groups responsible for 4e reduction process, degradation enhanced the amount of hydrogen peroxide. Figure 5IV shows its maximum enhancement to 14% H_2O_2 (n=3.7). It is known that the edge plane nitrogen quaternary functionalities and pyridinic sites catalyze four-electron pathways, while quaternary sites far from edges catalyze a two-electron pathway via a H_2O_2 intermediate. This study further improves the understanding of the specific role of nitrogen functionalities for ORR processes and presents a method for preparing a single active site system.

4. CONCLUSIONS

This study has demonstrated that potential cycling of iron-inserted N-doped carbon in a wide potential window in sulfuric acid then in alkaline solution under an oxidative atmosphere, eliminates the iron compounds, pyridinic and pyrrolic functional groups and leaves graphitic nitrogen as the only active site. This subtractive method for the first time presents a way to

synthesis a single active site catalyst to investigate its impact in ORR. By correlating XPS data, poisoning Fe-N_x active site method, with ORR measurements, we conclude that graphitic nitrogen, provides high catalytic activity for ORR, which is only slightly lower than the pyridinic containing catalyst in accordance to the earlier theoretically computation. RRDE measurements support the idea that the most quaternary nitrogen functionalities and pyridinic sites catalyze 4-e pathways, for the ORR.

ACKNOWLEDGMENT

This work was financially supported by NovEED project. Dr. Zabeada Aslam, from University of Leeds for TEM imaging, Dr Jose Portoles for recording XPS spectrum and Mrs. Maggie White from Newcastle University for recording X-ray diffractograms are acknowledged.

Appendix A. Supplementary data

The following are Supplementary data to this article:

XPS Survey spectra of the as-synthesized and degraded ink catalysts, Fe 2pXPS spectra of Fe 2p region of degraded catalyst ink,RRDE voltammetric responses of 20% Pt/C before (red line) and after degradation

AUTHOR INFORMATION

Corresponding Author

*E-mail: Maryam.bayati@ncl.ac.uk

Notes

The authors declare no competing financial interest.

REFERENCES

[1] A) S. J.Davis, K. Caldeira, H. D. Matthews *Science329*(**2010***)*1330. B) M. R. Raupach, S. J. Davis, G. P. Peters, R. M.Andrew, J. G.Canadell, P.Ciais, P. Friedlingstein, F. Jotzo, D. P. van Vuuren, C. Le Quéré, *Nat. Clim. Change 4(***2014**) 873.

[2] Z. Chen, D. Higgins, A. Yu, L. Zhang, J. Zhang *Energy Environ. Sci.*, *4*(**2011**) 3167.

[3] R. A. Jasinski*Nature 201 (***1964***)* 1212-1213.

[4] A) G.Wu, K. L.More, C. M.Johnston, P. Zelenay*Science332* (**2011**) 443. B) H. T.Chung, J.H.Won, P. Zelenay *Nat. Commun*. (**2013**) doi:10.1038/ncomms2944 C) L.Feng, L.Yang, Z. Huang, J.Luo, M.Li, D.Wang, Y. Chen, *Sci. Reports (***2013**) DOI: 10.1038/srep03306. D) M. Lefevre, E. Proietti, FJaouen, J.P. Dodelet, *Science324 (***2009**) 71. E) E. Proietti, F. Jaouen, M. Lefèvre, N. Larouche, J. Tian, J. Herranz, J. P. Dodelet, *Nat. Commun. 2 (***2011**) 416. F) Y. Li, W. Zhou, H. Wang, L. Xie, Y. Liang, F. Wei, J. C. Idrobo, S. J.Pennycook, Dai, H. *Nat. Nano.7 (***2012**) 394. G) Z.Chen, D.Higgins, H.Tao, R. S.Hsu, Z. W. Chen*J. Phys. Chem. C 113 (***2009**) 21008. H) S.Kundu, T. C.Nagaiah, W. Xia, Y. Wang, S. Van Dommele, J. H.Bitter, M. Santa, G. Grundmeier, M. Bron, W. Schuhmann, M. Muhler *J. Phys. Chem. C 113(***2009**) 14302.

[5] A) E. F. Holby, G. Wu, P. Zelenay, C. D. Taylor*J. Phys. Chem. C118(***2014**) 14388. B) G. L. Chai, Z., Hou, D. J.Shu, T.Ikeda,K. Terakura, *J. Am. Chem. Soc.136 (***2014)** 13629. C) K.Gong,F. Du, Z.Xia, M.Durstock, L. Dai*Science 323***(2009)** 760. D) H. Niwa, K. Horiba, Y. Harada, M. Oshima, T. Ikeda, K. Terakura, J. Ozaki, S. Miyata *J. Power Sources187 (***2009)** 93. E) J. B.Yang, D. J.Liu, N.N.Kariuki, L. X. Chen*Chem. Commun*.3(**2008**)329. F) K. Wan, Z. Yu, X. Li, M. Liu, G. Yang, J. Piao, Z. Liang *ACS Catal. 5 (***2015)** 4325−4332.G) Q.Li, B. W.Noffke, Y. Wang, B. Menezes, D. G. Peters, K. Raghavachari, L. Li *J. Am. Chem. Soc. 136 (***2014)** 3358. H) A. Zitolo, V. Goellner, V. Armel, M. T.Sougrati, T. Mineva, L. Stievano, E. Fonda, F. Jaouen *Nature Mater. 14(***2015)** 937. I) W. J. Jiang, L. Gu, L. Li, Y. Zhang, X. Zhang, L. J. Zhang, J. Q. Wang, J. S. Hu, Z. Wei, L. J. Wan*J. Am. Chem. Soc.138***(2016)** 3570. J) M. S. Thorum, J. M. Hankett, A. A. Gewirth *J. Phys. Chem. Lett. 2***(2011)** 295. K) K. Mamtani, U. S. Ozkan *Catal. Lett. 145***(2015)** 436. L)Q. Wang, Z. Y. Zhou, Y. J. Lai, Y. You, J. G. Liu, X. L. Wu, E. Terefe, C. Chen, L. Song, M. Rauf, N. Tian, S. G. Sun *J. Am. Chem. Soc.136***(2014)**10882. M) C. H. Choi, C. Baldizzone, G. Polymeros, E. Pizzutilo, O. Kasian, A. K. Schuppert, N. R. Sahraie, M. T. Sougrati, K. J.J. Mayhofer, F. Jaouen *ACS Catal.6***(2016)** 3136.N) D. Guo, R. Shibuya, C. Akiba, S. Saji, T. Kondo, J. Nakamura *Science 351***(2016)** 361.O) Y,Jiang, L. Yang, T. Sun, J. Zhao, Z.Lyu, O.Zhuo,

X. Wang, Q. Wu, J. Ma, Z. Hu *ACS Catal.*5 (**2015**) 6707.P) K. Xie, X. Qin, X. Wang, Y. Wang, H. Tao, Q. Wu, L. Yang, Z. Hu *Adv. Mater.* 24 (**2012**) 347.

[6] A) V.V. Strelko, V. S. Kuts, P.A. Thrower *Carbon 38 (***2000)** 1499. B) W. A. Saidi *J. Phys. Chem. Lett*. *4*(**2013)** 4160. C) W. Li, J. Wu, D. C. Higgins, J. Y.Choi, Z. Chen *ACS Catal*. 2 (**2012)** 2761-2768.D) U. Tylus, Q. Jia, K. Strickland, N. Ramaswamy, A. Serov, P. Atanassov, S. Mukerjee *J. Phys. Chem. C 118 (***2014)** 8999. E) W.Liang, J.Chen, Y.Liu, S. Chen *ACS Catal*. 4 (**2014)** 4170. F) K. Strickland, E. Miner, Q. Jia, U. Tylus, N. Ramaswamy, W. Liang, M. Sougrati, F. Jaouen, S. Mukerjee *Nature Commun*.(**2015)** DOI: 10.1038/ncomms8343.

[7] A) Y. Qiu, L. Gao *Chem. Commun*. (**2003)** 2378. b) X.Jin, V. V. Balasubramanian, S. T. Selvan, D. P. Sawant, M A. Chari; G. Q.Lu,A. Vinu, *Angew. Chem. Int. Ed.48 (***2009)** 7884.

[8] B. Y.Yu, S. Y. Kwak *J. Mater. Chem*. 20(**2010)** 8320.

[9] Z. Sheng, L. Shao, J. Chen, W. Bao, F. Wang, X. Xia*ACS Nano 5(***2011)** 4350.

[10] A) J. Du, F. Cheng, S. Wang, T. Zhang, J. Chen*Sci. Reports***, (2014)**DOI: 10.1038/srep04386. B) B. Kumar, M. Asadi, D. Pisasale, S. Sinha-Ray, B. A. Rosen, R. Haasch, J. Abiade, L.A. Yarin, A. Salehi-Khojin *Nature Commun*.(**2014)** DOI: 10.1038/ncomms3819. C) H. Peng, Z. Mo, S. Liao, H. Liang, L. Yang, F. Luo, H. Song, Y. Zhong, B. Zhang *Sci. Reports (***2013)** DOI: 10.1038/srep01765. D) K. Artyushkova, B. Kiefer, B. A. Halevi, Knop-Gericke, R. Schlogl, P. Atanassov *Chem. Comm*. 49(**2013)** 2539.

[11] S. A. Steiner, T. F.Baumann, J.Kong, J. H.Satcher, M. S. Dresselhaus, *Langmuir 23 (***2007)** 5161.

[12] A) T.Xing, Y.Zheng, L. H. Li, B. C. C. Cowie, D. Gunzelmann,S. Z. Qiao, S. Huang, Y. Chen, *ACS Nano 8 (***2014)** 6856. B) A. Dorjgotov, J.OK, Y. Jeon, S. H.Yoon, Y. J. Shul*J. Appl. Electrochem* 43 (**2013)** 387.

[13] A) J. G. Robke and E. J. Behrman, *J. Chem. Soc. D* **(1971)** 2867. B) X. Ge, A. Sumboja, D. Wuu, T. An, B.Li, F. W. T.Goh, T. S. A. Hor, Y. Zong, Z. Liu *ACS Nano 5(***2015)** 4643. C) Q. Zhu, S. L. Money, A. E. Russell, K. M. Thomas Langmuir 13 (1997) 2149.

[14] A) P. H.Matter, L.Zhang, U. S. Ozkan*J. Catal*. 239 (**2006)**83. B) N. P. Subramanian, X. Li, V. Nallathambi, S. P. Kumaraguru, H. Colon-Mercado, G. Wu, J. W. Lee, B. Popov *J. Power Sources 188(***2009)** 38.

[15] L.Lai, J. R.Potts, D.Zhan, L.Wang, C. K. Poh, C. Tang, H. Gong, Z. Shen, J. Lin, R. S. Ruoff *Energy Environ. Sci. 5 (***2012)** 7936.

[16] T. Sharifi, G.Hu, X. Jia, T. Wa°gberg *ACS Nano 6(***2012)** 8904.

Table of Contents Graphic and Synopsis

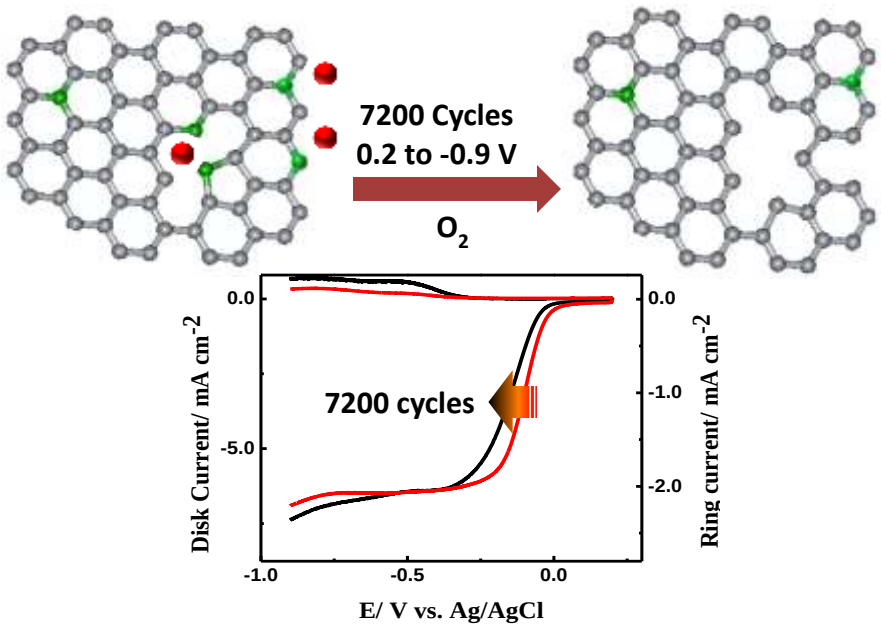

Appendix A.

Synthesis and Activity of A Single Active Site N-doped Electro-catalyst for Oxygen Reduction

Maryam Bayati*,Keith Scott

School of Chemical Engineering & Advanced Materials, Newcastle University, Newcastle upon Tyne, UK

Table S1. XPS functional group analysis of the N 1s region in synthesized and degraded catalysts. Total N atomic percentage in each sample is reported in the first column.

N Functional Group	Total N	Pyridinic	Quaternary	Pyrrolic	N-O
%Atom in as-synthesized catalyst	3.77	35.35	24.56	28.87	11.22
%Atom in degraded catalyst	2.14	0	67.67	0	32.33

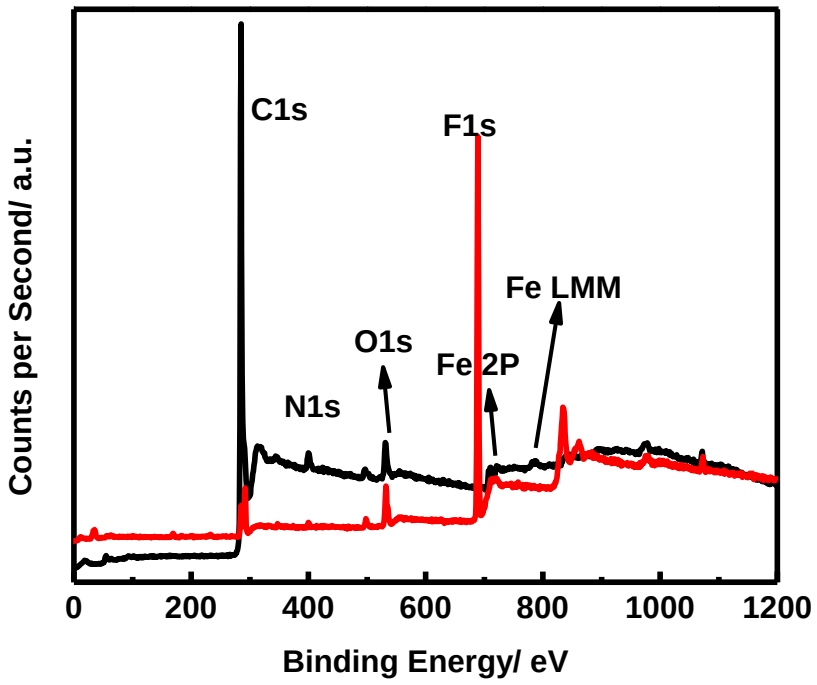

S2.XPS Survey spectra of the as-synthesized (black line) and degraded ink catalysts (red line). Y axis presents different scales for the spectra.

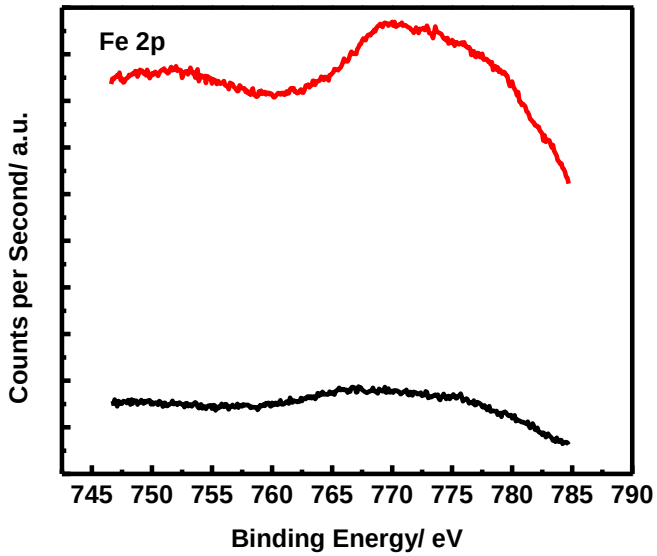

S3. Fe 2p XPS spectra of degraded catalyst ink (black line) and carbon-nafion mixture (Red line).

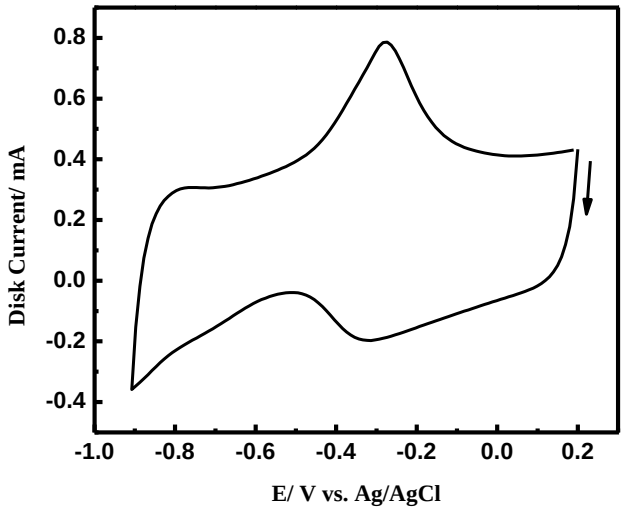

S4. Polarization curve of as-synthesized catalyst in 0.1 M NaOH solution and under nitrogen atmosphere. (Scan rate= 200 mVs^{-1})

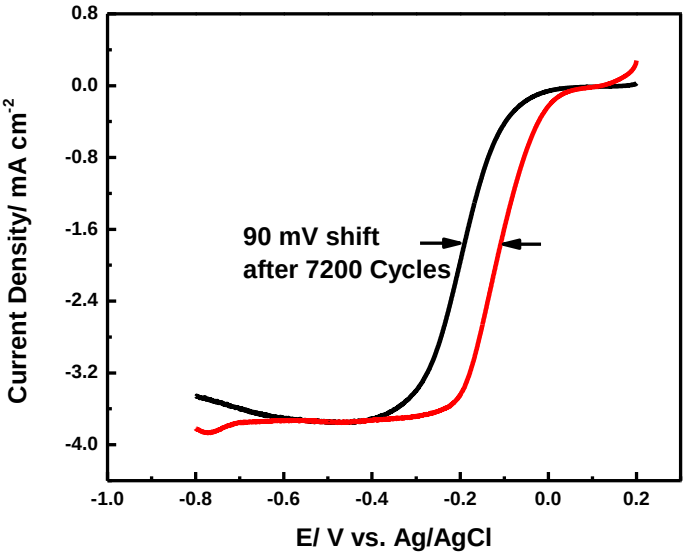

S5. RRDE voltammetric responses of 20% Pt/C for ORR in oxygen saturated solution of 0.1 M NaOH before (red line) and after degradation (black line) (scan rate=10 mVs^{-1}, rotation speed= 2500 rpm).

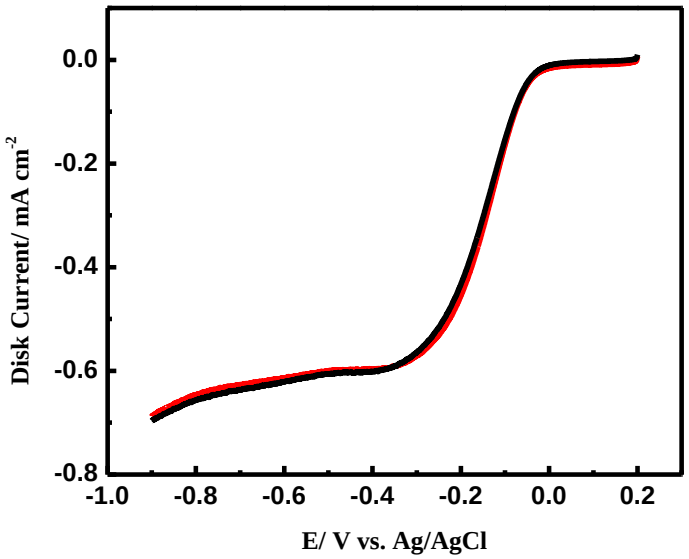

S6. RRDE voltammetric responses of degraded catalyst for ORR in oxygen saturated solution of 0.1 M NaOH (red line) and in 10 mM KCN + 0.1 M NaOH (black line) (scan rate=10 mVs^{-1}, rotation speed= 2500 rpm).